NANO EXPRESS   **Open Access**

CrossMark

Theoretical Study on Carrier Mobility of Hydrogenated Graphene/Hexagonal Boron-Nitride Heterobilayer

Zhenqiang Ye, Hua Geng[*] and Xiaoping Zheng[*]

Abstract

Hydrogenated graphene (HG)/hexagonal boron nitride (h-BN) heterobilayer is an ideal structure for the high-performance field effect transistor. In this paper, the carrier mobilities of HG/h-BN heterobilayer are investigated based on the first-principles calculations by considering the influence of stacking pattern between HG and h-BN, hydrogen coverage and hydrogenation pattern. With the same hydrogenation pattern, the electron mobility monotonously decreases when the hydrogen coverage increases. With the same hydrogen coverage, different hydrogenation patterns lead to significant changes of mobility. For 25% and 6.25% HGs, the μ_e (ΓK) of 25% pattern I is 8985.85 cm^2/(V s) and of 6.25% pattern I is 23,470.98 cm^2/(V s), which are much higher than other patterns. Meanwhile, the h-BN substrate affects the hole mobilities significantly, but it has limit influences on the electron mobilities. The hole mobilities of stacking patterns I and II are close to that of HG monolayer, but much lower than that of stacking patterns III and IV.

Keywords: Hydrogenated graphene, Hexagonal boron nitride, Effective mass, Carrier mobility

Introduction

Hydrogenated graphene (HG) [1, 2] is one of the most promising graphene-based materials. It has aroused widespread attention due to its extensive applications, such as hydrogen storage [3], ferromagnetism [4], fluorescence [5], and thermal rectification [6]. In contrast to metallic graphene, HG is predicted to be the semiconductor with a tunable band gap [7, 8]. Thus, it can be used as the channel material of field-effect transistor (FET) [9]. Excellent FETs should have an ultra-high carrier mobility of the channel material. As is well known, the traditional SiO_2 substrate has a significant negative effect on FET performance [10]. Recently, the studies show that monolayer hexagonal boron nitride (h-BN) [11, 12] is a promising candidate for the substrate of graphene-based FET. Monolayer h-BN and HG are lattice-matched structures, indicating a better contact performance. Hence, HG/h-BN heterobilayer is an ideal structure of the FET's channel. Unfortunately, there are only a few related studies about the electronic properties

of HG/h-BN heterobilayer structure. The carrier mobility performance of HG/h-BN heterobilayer is still an open question.

Most of the current studies on HG are devoted to engineering the desired electronic properties via hydrogenation [13–18]. Gao et al. [13] studied the hydrogen coverage and configuration dependence of the band gap of HG. Sahin et al. [14] compared the effect of adatom-patterned (hydrogenation) and hole-patterned (removal of carbon atom) graphene nanomeshes on band structure. Shkrebtii et al. [15] investigated the band structure of HG, where the structure of HG is limited in $C_{16}H_n$ system ($n = 0,2,8,16$). Song et al. [16] calculated the band gap of HGs with different hexagon vacancies. Bruzzone et al. [17] calculated the mobilities of HG with different hydrogen coverage (100%, 75%, 25%) by ab-initio simulations and found 25% HG got the highest mobility. There are also some studies about applying the hydrogenation in h-BN. Chen et al. [19] utilized the hydrogenation to realize semiconductor to metal transition in h-BN. Liang et al. [20] studied the interactions between 100% HG and 100% hydrogenated h-BN. It shows that the electron mobility of HG/hydrogenated h-BN is

* Correspondence: genghua@tsinghua.edu.cn; asean@mail.tsinghua.edu.cn
Department of Automation, Tsinghua University, Beijing 100084, People's Republic of China

only 50 cm^2/(V s) which is far away from that of graphene.

In a word, the current studies on the carrier mobility of HG/h-BN heterobilayer are still not enough. The main factors which affect the carrier mobility of HG/h-BN heterobilayer, namely hydrogen coverage, hydrogenation pattern and the stacking pattern between HG and h-BN, should be clarified. In this paper, the carrier mobilities of HG/h-BN heterobilayer structures were investigated based on the first-principles calculations. Firstly, the effect of the h-BN substrate on the mobilities of HG was investigated. Secondly, the electronic properties of HG with different hydrogen coverage were compared. Finally, different hydrogenation patterns were applied in 25% and 6.25% HG to reveal the influence of hydrogenation pattern.

Methods

All calculations were implemented in Atomistix ToolKit (ATK) [21] based on the density functional theory (DFT). The exchange correlation is the generalized gradient approximation (GGA) with the Perdew-Burke-Ernzerhof (PBE) functional. Van der Waals (vdW) correction adopted Grimme DFT-D2 method [22] for the heterobilayer structures. The cell length in z direction (perpendicular to the HG plane) is 20 Å, in order to eliminate the effect of its periodic images. The k-point sampling is $33 \times 33 \times 1$ Monkhorst-Pack grid.

Deformation potential approximation (DPA) method [23] is used to investigate the carrier mobility; the expression of the carrier mobility of 2D material [24, 25] is:

$$\mu = \frac{e\hbar^3 C_{2D}}{k_B T m^* m_d E_1^2},\tag{1}$$

where e is the electron charge, $\hbar$ is reduced Planck constant, k_B is Boltzmann constant, T is the temperature (it is set to be 300 K in the cases), and C_{2D} is the elastic modulus of the propagation direction. E_1 is the deformation potential constant defined by $E_1 = \Delta V/(\Delta l/l_0)$. ΔV is the energy change under proper cell compression and dilatation. The change of the conduction band minimum (CBM) is used for electrons and the valence band maximum (VBM) for holes. l_0 is the lattice length in the transport direction and Δl is its deformation ($\Delta l/l_0$ is set to be $-0.01, -0.005, 0, 0.005, 0.01$). m^* is the effective mass in the transport direction, calculated by:

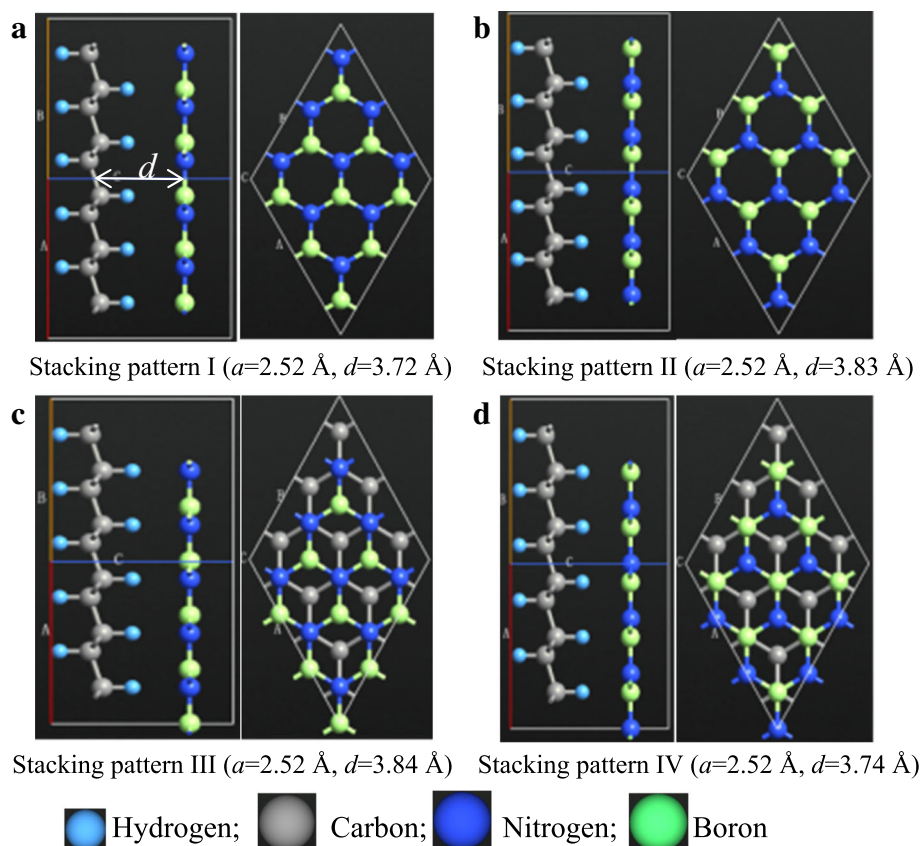$$m^* = \hbar^2 \left[\frac{\partial^2 E(k)}{\partial k^2} \right]^{-1},\tag{2}$$

where k is the wave vector and E is the energy. m_d is the equivalent density-of-state mass defined as $m_d = (m_x m_y)^{0.5}$. Deformation potential constant and effective

mass can be deduced from band structures, while the elastic modulus is extracted from phonon dispersion relations. It should be emphasized that the DPA method may overestimate the mobilities of arsenene, antimonene [26], and silicene [27] because it does not consider the effect of flexural acoustic (ZA) phonons. Shuai et al. [28, 29] discussed the applicability of DPA and found that it can estimate the electronic properties of graphene and graphyne well. The ZA phonons play a minor role in electron-phonon interactions for two-dimensional carbon materials. The electronic mobility of graphene [28] at room temperature is estimated to be 3.4×10^5 cm^2/(V s) by DPA method and 3.2×10^5 cm^2/(V s) [28] by considering all the electron-phonon interactions. As for HG, we will reanalyze the effect of ZA phonons in the next part.

Results and Discussion

Firstly, different stacking patterns between h-BN and HG were investigated, where the HG is 100% hydrogenated. It should be emphasized that the interaction between HG and h-BN is vdW force, which is far weaker than covalent bond. Hence, it is unnecessary to analyze the other HG/h-BN heterobilayers. There are four possible stacking patterns for the heterobilayer, as seen in Fig. 1a–d, where "a" is lattice parameter and "d" is interlayer distance. The interlayer distance is defined as the distance between the geometrical centers of HG layer and h-BN layer, as marked in Fig. 1a. In patterns I and II, the two skeletons are in AA stacking, while in patterns III and IV are in AB stacking. The structures were geometry optimized by the LBFGS optimizer method firstly. The convergence criteria for force tolerance are less than 0.001 eV/Å. After geometry optimization, the unit cell parameter is 2.52 Å for all the stacking patterns, while the interlayer distance depends on the stacking pattern. The interlayer distance of pattern I is the lowest, and pattern III is the highest. The vdW corrections of the four patterns are -651.69 meV, -658.14 meV, -658.22 meV, and -651.54 meV, respectively. Obviously, the tendency of vdW interaction coincides with that of the interlayer distance.

Band structure is one of the most important electronic properties. The corresponding band structures of stacking patterns I–IV are shown in Fig. 2. The two bold lines in each figure represent the bands including CBM (up) and VBM (down), respectively. Γ (0,0,0), M (0,0.5,0), K (0.333,0.333,0) are the symmetry points in the Brillouin zone. The main band structure information, including direct band gap (DBG), indirect band gap (IBG), CBM, and VBM positions, should be noticed. Generally, the four patterns have similar band structures. For patterns I–IV, the CBM and VBM are at point K and Γ, respectively. Patterns I and IV have similar DBG (4.35 eV) and

a Stacking pattern I (a=2.52 Å, d=3.72 Å)

b Stacking pattern II (a=2.52 Å, d=3.83 Å)

c Stacking pattern III (a=2.52 Å, d=3.84 Å)

d Stacking pattern IV (a=2.52 Å, d=3.74 Å)

Hydrogen;   Carbon;   Nitrogen;   Boron

Fig. 1 a–d Possible stacking patterns of 100%-HG/h-BN heterobilayer

IBG (3.25 eV), while the DBG and IBG of patterns II and III are about 4.22 eV and 2.98 eV. By comparing their interlayer distance, it can be concluded that the stronger interlayer interaction leads to the wider band gap. It should be emphasized that the band structure of single layer h-BN is also calculated with PBE. The band gap of h-BN is 4.65 eV which agrees well with the value reported in [30]. Overall, the method is suitable for h-BN.

Secondly, the influences of hydrogen coverage and hydrogenation patterns are considered, whereas the influence of hydrogenation origins from the changing of covalent bonds, which is much stronger than vdW force. Hence, only HG monolayer is investigated in this part. The considered structures are shown in Fig. 3, where "●" and "◎"denote the carbon atoms bonded with hydrogen atom at different sides. For the sake of the stability of the whole structure, hydrogen atoms are evenly distributed on each side. For 100% HG, it only has one stable pattern. Twenty-five percent HG composed by 8C and 2H has three different patterns. For 6.25% HG, it has 32C and 2H in the primitive cell. Only two patterns of 6.25% HG are considered. As shown in Fig. 3b, c, two hydrogenated carbon atoms are adjacent to each other
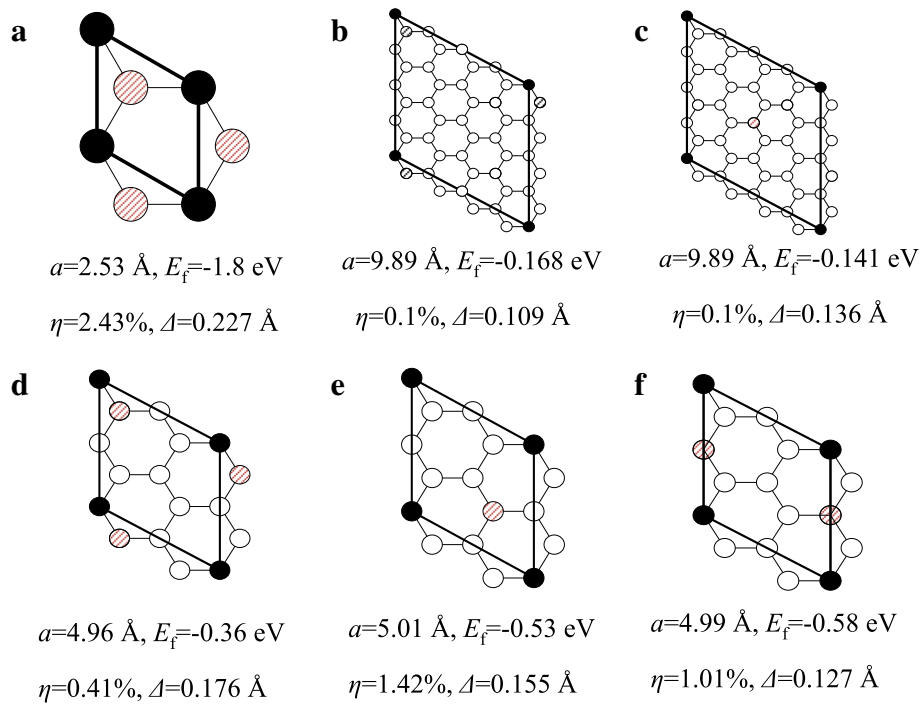
in pattern I and away from each other in pattern II. It should be noticed that 6.25% pattern I, 25% pattern I and 100% HG are the same type (two hydrogenated carbon atoms are adjacent). In Fig. 3, E_f is the formation energy per atom

$$E_f = \frac{E_{total} - n_H E_H - E_{graphene}}{n_H},\qquad (3)$$

where E_{total} is the total energy of HG, $E_{graphene}$ refers to the energy of pristine graphene, E_H is the energy per atom of the H_2 molecule, and n_H is the number of the adsorbed hydrogen atoms. E_f is used to check the stability of the structure, and the negative E_f suggests thermodynamics stability. The results in Fig. 3 imply that all the listed HGs are stable. η denotes the percentage rise of the lattice parameter of HG in contrast to graphene (the minimum unit cell length of graphene is 2.47 Å). On the whole, the lattice enhancement decreases with the decreasing hydrogen coverage. For 6.25% HG, η is almost negligible. Besides the hydrogen coverage, hydrogenation pattern also influences the lattice. For 25% HG, pattern I is enlarged least among the three patterns, mainly because the hydrogenated carbon atoms are adjacent. Δ is
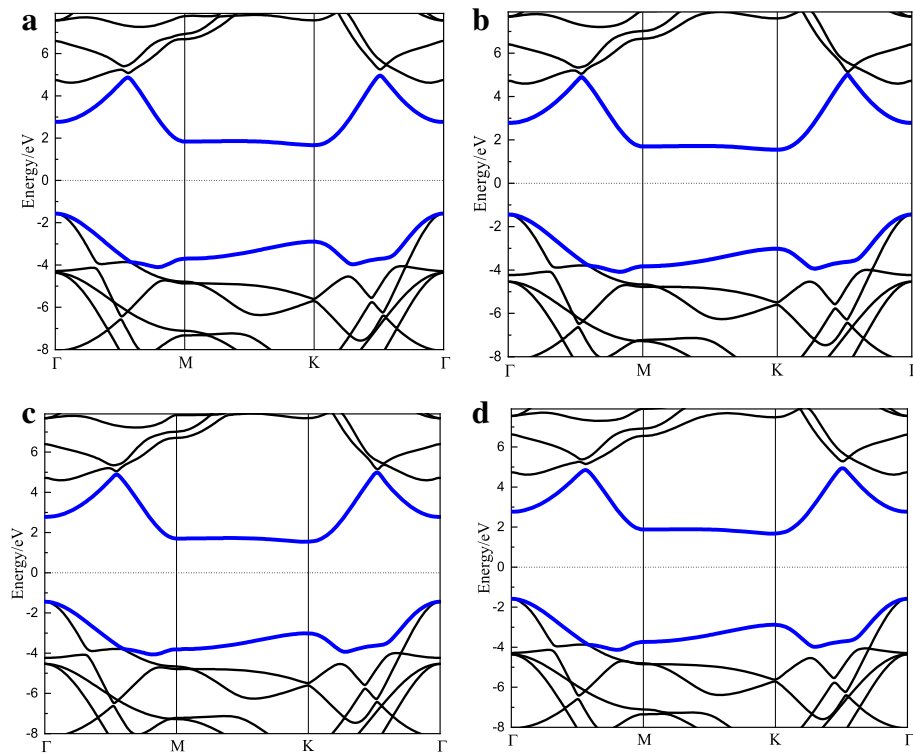
Fig. 2 a–d The band structures of 100%-HG/h-BN heterobilayer stacking patterns I–IV

a

a=2.53 Å, E_f=-1.8 eV

η=2.43%, Δ=0.227 Å

b

a=9.89 Å, E_f=-0.168 eV

η=0.1%, Δ=0.109 Å

c

a=9.89 Å, E_f=-0.141 eV

η=0.1%, Δ=0.136 Å

d

a=4.96 Å, E_f=-0.36 eV

η=0.41%, Δ=0.176 Å

e

a=5.01 Å, E_f=-0.53 eV

η=1.42%, Δ=0.155 Å

f

a=4.99 Å, E_f=-0.58 eV

η=1.01%, Δ=0.127 Å

Fig. 3 Schematic of primitive cell of HGs with different hydrogen coverage and pattern. **a** 100%. **b**, **c** 6.25% patterns I and II. **d**, **f** 25% pattern I–III

Ye *et al. Nanoscale Research Letters*   (2018) 13:376

Page 5 of 8

the buckling parameter, which is defined as the standard deviation of the out-of-plane displacements of the carbon atoms. Generally, the buckling parameter increases with the increased hydrogen coverage.

The band structures of the above HGs are shown in Fig. 4. The band gap of 100% HG is about 4.14 eV, in good agreement with the previous literature [16, 31]. For 25% HG, the band gap is strongly affected by the hydrogenation pattern. Pattern II has an IBG of 3.0 eV, while the IBG of pattern III is 0 eV. The IBG from zero to nonzero indicates a transition from metallic to semiconductor. In addition, pattern II has different DBG and IBG, suggesting that its CBM and VBM are at different points. For 6.25% HG, the VBM and CBM are at the same points for both of the two patterns, which of pattern I is (0.153, 0.423, 0) and pattern II is (0.24, 0.24, 0). The band gap of two 6.25% HGs are 0 eV and 0.49 eV, both of which reduced significantly in contrast to that of 100% HG. Generally, both hydrogen coverage and hydrogenation patterns are effective methods to modulate band gap.

Table 1 presents the estimated values of elastic modulus C_{2D}, effective mass m^* and deformation potential constant E_1. C_{2D} and m^* are direction-dependent parameters. Among all the directions, ΓM and ΓK are the most

concerned. Hence, C_{2D} ($\Gamma M/\Gamma K$) and m^* ($\Gamma M/\Gamma K$) are listed in Table 1. $C_{2D} = \rho v_g^2$, where ρ is the density and v_g denotes group velocity of acoustic phonon. Because hydrogenation has few effects on group velocity, C_{2D} of different HGs are similar with each other. The HG v_g is about 23 km/s in ΓK direction and 19.4 km/s in ΓM, so C_{2D} (ΓK) is much higher than C_{2D} (ΓM). The deformation potential constant has no regular tendency with the different patterns. Generally, the vdW interaction between HG and h-BN increases the deformation potential constant.

Effective mass is more complicated, since it depends on carrier and direction. There are three points that should be noted on effective mass. First, the electron effective mass of 100% HG and 100%-HG/h-BN heterobilayer are isotropic, i.e., $m^*(\Gamma M) = m^*(\Gamma K)$. The heterobilayer structure leads to a slight drop of electron effective mass compared with 100% HG monolayer. The stacking pattern has slight influence on the electron effective mass (all of the four stacking patterns are about 0.90). Second, under the same hydrogenation pattern (i.e., 100%, 25% pattern I and 6.25% pattern I), the electron $m^*(\Gamma K)$ decreases with the decreased hydrogen coverage. It is shown that the limit is 0.024 (the effective mass of graphene) as the hydrogen coverage reduces to zero. Third, under the same hydrogen
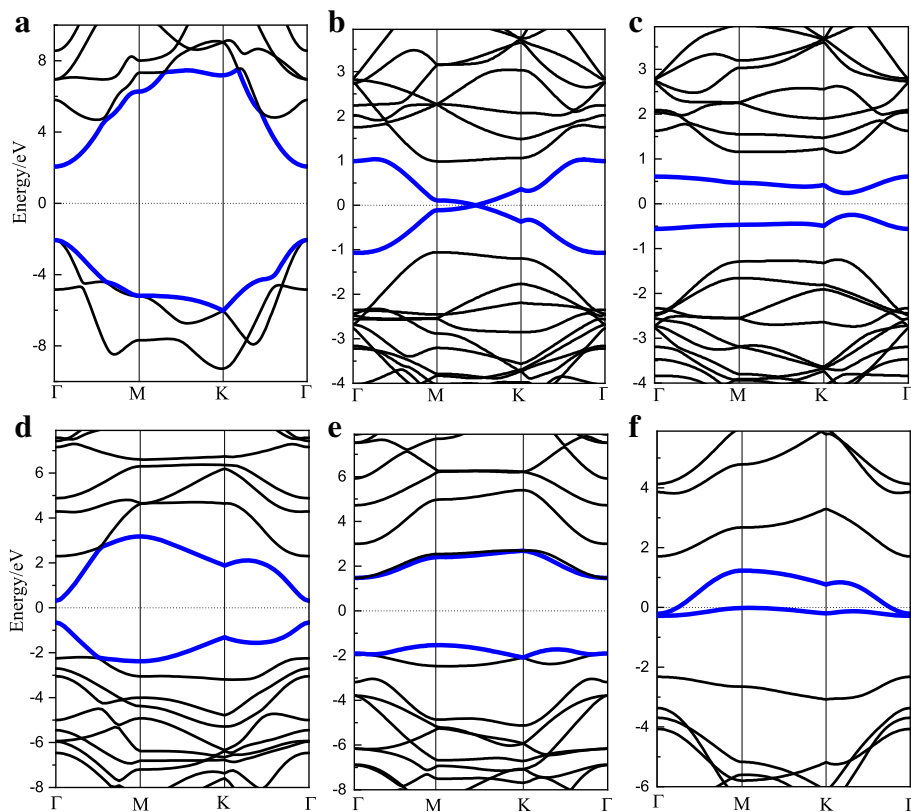
Fig. 4 Band structures of HGs. **a** 100%. **b**, **c** 6.25% pattern I and II. **d**, **f** 25% pattern I–III

Ye *et al. Nanoscale Research Letters* (2018) 13:376

Page 6 of 8

Table 1 The elastic modulus C_{2D}, effective mass m^*, and deformation potential constant E_1. "m_0" denotes the electron mass 9.109×10^{-31} kg

Type	Pattern	C_{2D}, N/m		m^*, m_0		E_1, eV
		(ΓM)	(ΓK)	(ΓM)	(ΓK)	
Electron	100%	350.59	475.98	0.967	0.967	9.16
	25% pattern I	337.43	500.41	0.468	0.087	8.22
	25% pattern II	333.96	504.63	1.609	1.096	7.91
	25% pattern III	339.15	504.63	1.941	0.545	7.49
	6.25% pattern I	335.42	502.06	0.491	0.055	7.1
	6.25% pattern II	335.67	502.06	0.169	0.215	6.76
	Stacking pattern I	338.80	459.97	0.881	0.881	10.5
	Stacking pattern II	338.80	459.97	0.901	0.901	9.81
	Stacking pattern III	338.80	459.97	0.884	0.884	9.92
	Stacking pattern IV	338.80	459.97	0.905	0.905	9.45
Hole	100%	350.59	475.98	0.627	0.703	9.40
	25% pattern I	337.43	500.41	2.851	0.101	8.15
	25% pattern II	333.96	504.63	1.071	1.884	8.2
	25% pattern III	339.15	504.63	5.201	2.356	8.1
	6.25% pattern I	335.42	502.06	0.057	0.495	7.72
	6.25% pattern II	335.67	502.06	0.179	0.219	7.55
	Stacking pattern I	338.80	459.97	0.62	0.641	10.5
	Stacking pattern II	338.80	459.97	0.62	0.714	9.81
	Stacking pattern III	338.80	459.97	0.259	0.294	9.92
	Stacking pattern IV	338.80	459.97	0.26	0.282	9.45

coverage, effective mass is also affected by hydrogenation pattern. For 25% HG, the electron effective mass of pattern I is much lower than the other two. In a word, the effective mass is more likely to be affected by hydrogenation but not the elastic modulus and deformation potential constant.

Table 2 The electron and hole mobilities in ΓM and ΓK direction. The subscripts "e" and "h" refer to electron and hole, respectively. Unit is cm^2/(V s)

	μ_e (ΓM)	μ_h (ΓM)	μ_e (ΓK)	μ_h (ΓK)
100%	95.18	162.71	129.22	197.02
25% pattern I	1126.39	70.73	8985.85	2960.80
25% pattern II	53.21	69.54	118.03	59.73
25% pattern III	64.50	6.05	341.81	19.86
6.25% pattern I	1756.48	12,520.27	23,470.98	2158.01
6.25% pattern II	4856.81	3539.15	5710.03	4326.59
Stacking pattern I	84.33	167.47	114.49	219.91
Stacking pattern II	92.37	181.78	125.41	214.30
Stacking pattern III	93.84	1026.06	127.40	1227.19
Stacking pattern IV	98.66	1147.82	133.95	1436.75

In Table 2, the electron and hole mobilities are computed based on the above parameters. Because the effective mass is more likely to be affected, the tendency of mobility is similar with that of effective mass. Generally speaking, hydrogenation dramatically reduces the mobility of graphene. The theoretical mobility of graphene (3.2×10^5 cm^2/(V s)[28]) is several orders of magnitude higher than that of HG. In addition, HGs have asymmetric ($\mu_e \neq \mu_h$) and anisotropic ($\mu(\Gamma M) \neq \mu (\Gamma K)$) mobilities. There are three details that should be noticed. First, under the same hydrogenation pattern, the electron mobility monotonously decreases with the increasing hydrogen coverage. But, if under different hydrogenation pattern, the conclusion is not always established. For example, the mobilities of 25% pattern II are lower than that of 100% HG. Second, for 25% and 6.25% HGs, pattern I has a higher μ_e compared to the other patterns. The μ_e (ΓK) of 25% pattern I is 8985.85 cm^2/(V s) and of 6.25% pattern I is 23,470.98 cm^2/(V s), much higher than black phosphorene [24] and MoS_2 [32]. Third, the h-BN substrate affects the hole mobilities significantly, while it has little effect on the electron mobilities. It indicates the hole mobilities of stacking patterns I and II are close to that of HG monolayer, but much lower than that of stacking patterns III and IV. Hence, different stacking patterns have significant effects on hole mobilities but little effects on electron mobilities.

Moreover, the mobility of 100% HG was recalculated by considering all the electron-phonon interactions, namely longitude acoustic (LA), transverse acoustic (TA) and ZA phonons. The results show that the electron mobility is 105 cm^2/(V s) in ΓK direction. Figure 5 gives the electron-phonon interaction matrix elements |g| of LA, TA and ZA phonons. It shows that the LA phonons dominate in electron-phonon interactions. On the whole, LA phonons have larger interaction strength with electrons compared with the TA and ZA phonons. Although the mobility value is slightly lower than that calculated by DPA method, the difference of two methods in HG is much less than that in arsenene, antimonene, and silicene. Generally, the DPA method is feasible in our study.

Conclusions

In summary, the carrier mobilities of HG/h-BN heterobilayer were investigated based on the first-principles calculations in this paper. The influence on mobilities is discussed in terms of the stacking patterns of HG/h-BN heterobilayer, hydrogen coverage, and hydrogenation pattern. The elastic modulus C_{2D}, effective mass m^*, and deformation potential constant E_1 are calculated to analyze the mobilities. The deformation potential constant has no regular tendency with the different patterns.
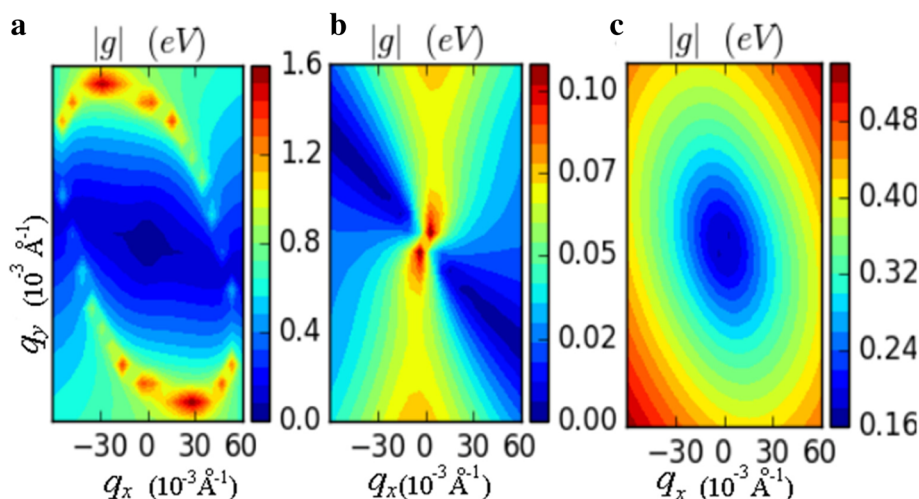
Fig. 5 The electron-phonon interaction matrix elements $|g|$ of **a** LA, **b** TA, and **c** ZA phonons

The elastic modulus and the effective mass in HGs are direction-dependent. The results show that ΓK direction has a higher elastic modulus. The effective mass is more likely to be affected by different hydrogenations and stacking patterns. Under the same hydrogenation pattern, the electron mobility monotonously decreases with the increasing hydrogen coverage. Under the same hydrogen coverage, different patterns lead to a significant change of mobilities. For 25% and 6.25% HGs, the μ_e (ΓK) of 25% pattern I is 8985.85 $cm^2/(V\,s)$ and of the μ_e (ΓK) 6.25% pattern I is 23,470.98 $cm^2/(V\,s)$; both are much higher than the other patterns. As for the influence of h-BN substrate, different stacking patterns affect the hole mobilities significantly, but hardly affect the electron mobilities. The hole mobilities of stacking patterns I and II are close to that of HG monolayer, but much lower than that of stacking patterns III and IV. Overall, HG/h-BN heterobilayer has a considerable carrier mobility and band gap under a specific hydrogenation pattern, which has promising application prospects in electronics and photonics.

Abbreviations
ATK: Atomistix ToolKit; CBM: Conduction band minimum; DBG: Direct band gap; DFT: Density functional theory; DPA: Deformation potential approximation; FET: Field-effect transistor; GGA: Generalized gradient approximation; h-BN: Hexagonal boron nitride; HG: Hydrogenated graphene; IBG: Indirect band gap; PBE: Perdew-Burke-Ernzerhof; VBM: Valence band maximum; vdW: van der Waals

Availability of Data and Materials
The datasets supporting the conclusions of this paper are included in the main text, figures, and tables.

Authors' Contributions
ZY carried out the ATK simulations and drafted the manuscript. HG assisted in the data analysis and the manuscript writing and revision. XZ supported and supervised the whole research. All the authors discussed the results and approved the final manuscript.

Competing Interests
The authors declare that they have no competing interests.

Publisher's Note
Springer Nature remains neutral with regard to jurisdictional claims in published maps and institutional affiliations.

References
1. Elias DC, Nair RR, Mohiuddin TMG et al (2008) Control of graphene's properties by reversible hydrogenation. Science 323(5914):610–613.
2. Zhou C, Chen S, Lou J et al (2014) Graphene's cousin: the present and future of graphane. Nanoscale Res Lett 9(1):26.
3. Hussain T, Sarkar AD, Ahuja R (2014) Functionalization of hydrogenated graphene by polylithiated species for efficient hydrogen storage. Int J Hydrogen Energ 39(6):2560–2566.
4. Zhou J, Wang Q, Sun Q, Chen XS, Kawazoe Y, Jena P (2009) Ferromagnetism in semihydrogenated graphene sheet. Nano Lett 9(11): 3867–3870.
5. Schäfer RA, Englert JM, Wehrfritz P et al (2013) On the way to graphane-pronounced fluorescence of polyhydrogenated graphene. Angew Chem Int Ed 52(2):754–757.
6. Rajabpour A, Allaei SMV, Kowsary F (2011) Interface thermal resistance and thermal rectification in hybrid graphene-graphane nanoribbons: a nonequilibrium molecular dynamics study. Appl Phys Lett 99(5):666–670.

7. He H, Pan B, Argyraki A et al (2014) Advances in wide bandgap SiC for optoelectronics. Eur Phys J B 87(3):58–87.
8. Son J, Lee S, Kim SJ et al (2016) Hydrogenated monolayer graphene with reversible and tunable wide band gap and its field-effect transistor. Nat Commun 7:13261.
9. Fiori G, Lebègue S, Betti A et al (2010) Simulation of hydrogenated graphene field-effect transistors through a multiscale approach. Phys Rev B 82(15):1462–1465.
10. Bartolomeo AD, Giubileo F, Iemmo L et al (2016) Side-gate leakage and field emission in all-graphene field effect transistors on SiO_2/Si substrate. Appl Phys Lett 109:023510.
11. Dean CR, Young AF, Meric I et al (2010) Boron nitride substrates for high-quality graphene electronics. Nat Nanotechnol 5(10):722–726.
12. Xue J, Sanchez-Yamagishi J, Bulmash D et al (2011) STM spectroscopy of ultra-flat graphene on hexagonal boron nitride. Nat Mater 10:282–285.
13. Gao H, Wang L, Zhao J, Ding F, Lu J (2011) Band gap tuning of hydrogenated graphene: H coverage and configuration dependence. J Phys Chem C 115(8):3236–3242.
14. Sahin H, Ciraci S (2011) Structural, mechanical, and electronic properties of defect-patterned graphene nanomeshes from first principles. Phys Rev B 84(3):035452.
15. Shkrebtii AI, Heritage E, McNelles P et al (2012) Graphene and graphane functionalization using hydrogen and nitrogen: electronic, optical and vibrational signatures. Phys Status Solidi 9(6):1378–1383.
16. Song EH, Ali G, Yoo SH, Jiang Q, Cho SO (2014) Tuning electronic and magnetic properties of partially hydrogenated graphene by biaxial tensile strain: a computational study. Nanoscale Res Lett 9(1):491–491.
17. Bruzzone S, Fiori G (2011) Ab-initio simulations of deformation potentials and electron mobility in chemically modified graphene and two-dimensional hexagonal boron-nitride. Appl Phys Lett 99:22108.
18. Samarakoon DK, Wang XQ (2010) Tunable band gap in hydrogenated bilayer graphene. ACS Nano 4(7):4126–4130.
19. Chen W, Li Y, Yu G et al (2010) Hydrogenation: a simple approach to realize semiconductor–half-metal–metal transition in boron nitride nanoribbons. J Am Chem Soc 132(5):1699–1705.
20. Liang Q, Jiang J, Meng R et al (2016) Tuning the electronic properties and work functions of graphane/fully hydrogenated h-BN heterobilayers via heteronuclear dihydrogen bonding and electric field control. Phys Chem Chem Phys 18(24):16386–16395.
21. Atomistix Toolkit version 2018.06, Synopsys QuantumWise A/S. (www.quantumwise.com).
22. Grimme S (2006) Semiempirical GGA-type density functional constructed with a long-range dispersion correction. J Comput Chem 27(15):1787–1799.
23. Shockley W, Bardeen J (1950) Energy bands and mobilities in monatomic semiconductors. Phys Rev 77(3):407–408.
24. Qiao J, Kong X, Hu ZX, Yang F, Ji W (2014) High-mobility transport anisotropy and linear dichroism in few-layer black phosphorus. Nat Commun 5:4475.
25. Gao S, Xiang H, Xu et al. Theoretical study of carrier mobility in two-dimensional tetragonal carbon allotrope from porous graphene. Chinese Phys Lett 2016; 33(8):083101.
26. Wang Y, Huang P, Ye M et al (2017) Many-body effect, carrier mobility, and device performance of hexagonal arsenene and antimonene. Chem Mater 29(5):2191–2201.
27. Gunst T, Markussen T, Stokbro K, Brandbyge M (2016) First-principles method for electron-phonon coupling and electron mobility: applications to two-dimensional materials. Phys Rev B 93:035414.
28. Xi JY, Nakamura Y, Zhao TQ, Wang D, Shuai ZG (2018) Theoretical studies on the deformation potential, electron-phonon coupling, and carrier transports of layered systems. Acta Phys -Chim Sin 34(9):961–976.
29. Xi JY, Long MQ, Tang L, Wang D, Shuai ZG (2012) First-principles prediction of charge mobility in carbon and organic nanomaterials. Nanoscale 4:4348–4369.
30. Topsakal M, Aktürk E, Ciraci S (2009) First-principles study of two-and one-dimensional honeycomb structures of boron nitride. Phys Rev B 79:115442.
31. Li Y, Li F, Chen Z (2012) Graphane/fluorographene bilayer: considerable C-H⋯F-C hydrogen bonding and effective band structure engineering. J Am Chem Soc 134(27):11269–11275.
32. Xiao J, Long M, Li X, Xu H, Huang H, Gao Y (2014) Theoretical prediction of electronic structure and carrier mobility in single-walled MoS_2 nanotubes. Sci Rep 4:4327.